

**Microbiology:**  
**Differential Virulence of *Candida glabrata*  
Glycosylation Mutants**

Lara West, Douglas W. Lowman, Héctor M. Mora-Montes, Sarah Grubb, Craig Murdoch, Martin H. Thornhill, Neil A.R. Gow, David Williams and Ken Haynes

*J. Biol. Chem.* 2013, 288:22006-22018.

doi: 10.1074/jbc.M113.478743 originally published online May 28, 2013

MICROBIOLOGY

GLYCOBIOLOGY AND  
EXTRACELLULAR MATRICES

Access the most updated version of this article at doi: [10.1074/jbc.M113.478743](https://doi.org/10.1074/jbc.M113.478743)

Find articles, minireviews, Reflections and Classics on similar topics on the [JBC Affinity Sites](http://www.jbc.org/).

Alerts:

- [When this article is cited](#)
- [When a correction for this article is posted](#)

[Click here](#) to choose from all of JBC's e-mail alerts

Supplemental material:

<http://www.jbc.org/content/suppl/2013/05/28/M113.478743.DC1.html>

This article cites 84 references, 36 of which can be accessed free at  
<http://www.jbc.org/content/288/30/22006.full.html#ref-list-1>

# Differential Virulence of *Candida glabrata* Glycosylation Mutants<sup>\*[5]</sup>

Received for publication, April 24, 2013, and in revised form, May 24, 2013. Published, JBC Papers in Press, May 28, 2013, DOI 10.1074/jbc.M113.478743

Lara West<sup>‡</sup>, Douglas W. Lowman<sup>§¶</sup>, Héctor M. Mora-Montes<sup>||\*\*</sup>, Sarah Grubb<sup>††1</sup>, Craig Murdoch<sup>††</sup>, Martin H. Thornhill<sup>††</sup>, Neil A.R. Gow<sup>||</sup>, David Williams<sup>§</sup>, and Ken Haynes<sup>‡§§2</sup>

From the <sup>‡</sup>Department of Microbiology, Imperial College London, London, SW7 2AZ, United Kingdom, the <sup>§</sup>Department of Surgery, Quillen College of Medicine, East Tennessee State University, Johnson City, Tennessee 37614, <sup>¶</sup>AppRidge International, LLC, Jonesborough, Tennessee 37659-0266, the <sup>||</sup>School of Medical Sciences, Institute of Medical Sciences, University of Aberdeen, Foresterhill, Aberdeen AB25 2ZD, United Kingdom, the <sup>\*\*</sup>Departamento de Biología, División de Ciencias Naturales y Exactas, Universidad de Guanajuato, Noria Alta s/n, Col. Noria Alta, Guanajuato, Gto. 36050, México, the <sup>††</sup>University of Sheffield School of Clinical Dentistry, Sheffield, S10 2TA, United Kingdom, and <sup>§§</sup>Biosciences, College of Life and Environmental Sciences, University of Exeter, Exeter, EX4 4QD, United Kingdom

**Background:** *Candida glabrata* virulence is poorly understood at the molecular level.

**Results:** Inactivation of components of the *C. glabrata* glycosylation machinery results in changes in fungal mannan structure and altered virulence.

**Conclusion:** Changes in *C. glabrata* cell wall architecture impact the host-pathogen interactions.

**Significance:** Greater understanding of *C. glabrata* virulence will provide insights that can be adopted for development of novel diagnostic and therapeutic interventions.

The fungus *Candida glabrata* is an important and increasingly common pathogen of humans, particularly in immunocompromised hosts. Despite this, little is known about the attributes that allow this organism to cause disease or its interaction with the host immune system. However, in common with other fungi, the cell wall of *C. glabrata* is the initial point of contact between the host and pathogen, and as such, it is likely to play an important role in mediating interactions and hence virulence. Here, we show both through genetic complementation and polysaccharide structural analyses that *C. glabrata* ANP1, MNN2, and MNN11 encode functional orthologues of the respective *Saccharomyces cerevisiae* mannosyltransferases. Furthermore, we show that deletion of the *C. glabrata* Anp1, Mnn2, and Mnn11 mannosyltransferases directly affects the structure of the fungal *N*-linked mannan, in line with their predicted functions, and this has implications for cell wall integrity and consequently virulence. *C. glabrata* *anp1* and *mnn2* mutants showed increased virulence, compared with wild-type (and *mnn11*) cells. This is in contrast to *Candida albicans* where inactivation of genes involved in mannan biosynthesis has usually been linked to an attenuation of virulence. In the long term, a better understanding of the attributes that allow *C. glabrata* to cause disease will provide insights that can be adopted for the development of novel therapeutic and diagnostic approaches.

The fungal pathogen *Candida glabrata* is a major cause of life-threatening disease in the immunocompromised patient population, causing up to 30% of all candidemias and having a higher attributable mortality than *Candida albicans* (1, 2). As with other pathogenic *Candida* species, the cell wall of *C. glabrata* is the point of contact between host and fungus. In addition, it performs many other functions, protecting the fungal cell from hostile environments, enabling adherence to host surfaces, and maintaining cell shape. The cell walls of *Saccharomyces cerevisiae* and *C. albicans* have both been investigated in detail and extensively reviewed in the literature (3–5). Common to many other fungi, the central core of their cell walls is a branched  $\beta$ -(1,3)-,  $\beta$ -(1,6)-glucan linked to chitin via a  $\beta$ -(1,4)-glucan linkage. This core structure is generally found close to the cell membrane, with chitin innermost, and the  $\beta$ -(1,6)-glucan structure/linkages displayed outwards acting as a linker to the outer cell wall mannoproteins. Some of the chitin and glucan chains extend throughout the entire depth of the cell wall structure (6, 7). The outer glycoprotein layer of the fungal cell wall plays a major role in host recognition (8–15).

These glycoproteins are decorated with both *N*- and *O*-linked sugars, principally mannans, the precise nature of which varies among species but can result in addition of up to 200 mannose units (16). Structural studies indicate that *C. glabrata* mannan is more closely related to that of *S. cerevisiae* than *C. albicans* (17–19), and it shows some inter-strain variation (20). Despite this variation in mannan structure, the core biosynthetic machinery appears to be relatively well conserved, a fact that facilitates the analysis of *C. glabrata* glycosylation. *N*-Linked protein glycosylation occurs in two stages. First, assembly of the core oligosaccharide structure takes place at the membrane of the endoplasmic reticulum (21). The completed core structure is a branched oligosaccharide of residues Glc<sub>3</sub>Man<sub>9</sub>GlcNAc<sub>2</sub>, which is transferred *en bloc* from its lipid

\* This work was supported, in whole or in part, by National Institutes of Health Grant RO1GM53522 from NIGMS (to D. L. W.). This work was also supported by Biotechnology and Biological Sciences Research Council Grant BBF005210 (to the Haynes Laboratory), Wellcome Trust Grants 072420 075174, and Wellcome Trust Grant 080088 (to the Gow Laboratory).

⌘ Author's Choice—Final version full access.

[5] This article contains supplemental Fig. 1.

<sup>1</sup> Supported by National Institutes of Health Grant R21 AI065549-01A1 from NIAID (to M. H. T.).

<sup>2</sup> To whom correspondence should be addressed: 325 Geoffrey Pope Bldg., Stocker Rd., Exeter, EX4 4QD, UK. Tel.: 01392-723434; E-mail: k.haynes@exeter.ac.uk.

**TABLE 1**  
Fungal strains used in this study

Species	Strain	Genotype or description	Source
<i>C. glabrata</i>	ATCC 2001	Wild type	ATCC
<i>C. glabrata</i>	ΔHT6	Δhis3::ScURA3 Δtrp1	48
<i>C. glabrata</i>	XFS-1	Δhis3::ScURA3 Δtrp1 Δanp1::HIS3	This study
<i>C. glabrata</i>	XFS-1P	Δhis3::ScURA3 Δtrp1 Δanp1::HIS3 pCgACT14 (TRP1)	This study
<i>C. glabrata</i>	LJW-5RLP	Δhis3::URA3 Δtrp1 Δanp1::ANP1 pCgACT14 (TRP1) pCgACH3 (HIS3)	This study
<i>C. glabrata</i>	LJW-2	Δhis3::URA3 Δtrp1 Δmnn2::HIS3	This study
<i>C. glabrata</i>	LJW-2P	Δhis3::URA3 Δtrp1 Δmnn2::HIS3 pCgACT14 (TRP1)	This study
<i>C. glabrata</i>	LJW-2RLP	Δhis3::URA3 Δtrp1 Δmnn2::MNN2 pCgACT14 (TRP1) pCgACH3 (HIS3)	This study
<i>C. glabrata</i>	LJW-3	Δhis3::URA3 Δtrp1 Δmnn11::HIS3	This study
<i>C. glabrata</i>	LJW-3P	Δhis3::URA3 Δtrp1 Δmnn11::HIS3 pCgACT14 (TRP1)	This study
<i>S. cerevisiae</i>	BY4741	MATa Δhis3 Δleu2 Δmet15 Δura3	51
<i>C. glabrata</i>	LJW-6	Δhis3::URA3 Δtrp1 Δanp1::HIS3 pLJW5 (TRP1 ScANP1)	This study
<i>S. cerevisiae</i>	LJW-8	MATa mnn2Δ::kanMX4 Δhis3 Δleu2 Δmet15 Δura3 pLJW7 (LEU2 CgMNN2)	This study
<i>S. cerevisiae</i>	L9	MATa mnn11Δ::kanMX4 Δhis3 Δleu2 Δmet15 Δura3 pLJW8 (LEU2 CgMNN11)	This study

anchor to the target asparagine residues on a nascent peptide (22). Once attached, the oligosaccharide is trimmed to leave Man<sub>8</sub>GlcNAc<sub>2</sub> (23). The second part of the *N*-linked glycosylation process occurs in the Golgi complex, where a single  $\alpha$ -(1,6)-linked mannose is added to Man<sub>8</sub>GlcNAc<sub>2</sub> core by Och1 (24). Proteins either then receive a core-type structure by the addition of two further mannoses or a much more highly decorated  $\alpha$ -(1,6)-linked backbone structure, branched by  $\alpha$ -(1,2)- and  $\alpha$ -(1,3)-mannoses (25, 26). In *S. cerevisiae* this process requires both the *MNN* and *KTR/KRE/MNT* families of mannosyltransferases, including Anp1, Mnn2, and Mnn11 (27–35). It is this final stage in processing that accounts for the huge diversity of glycans decorating fungal glycoproteins. Interestingly, many of these fungal mannosyltransferases are absent from human cells, and hence their analysis has potential with respect to the development of novel antifungal and immunotherapy.

With this in mind, the enzymes involved in both the processing of *N*- and *O*-linked mannans in *C. albicans* have been analyzed and shown to be required for the virulence of this organism, including those specifically involved in both *N*-glycosylation (36) and *O*-glycosylation (37, 38). In addition glycosylation appears to be important in mediating virulence in *Cryptococcus neoformans* (39, 40). Indeed, in *C. neoformans* the polysaccharide capsule that includes mannose-based components is essential for the virulence of this fungus (41). Furthermore, a heterogeneous group of mannoproteins are critical antigens in stimulating T cell responses (42). This importance in virulence may be due in part to differential host recognition. *N*- and *O*-linked mannans are major pathogen-associated molecular patterns and, along with  $\beta$ -glucans, play important roles in triggering host innate immunity. Recent findings in *C. albicans* have highlighted how a coordinated immune response, with stimulus from both *N*- and *O*-linked glycans of the mannoproteins, and also the  $\beta$ -glucan triggers the immune cascade (6). This underlines the fact that multiple components of the cell wall are involved in fungal recognition. Some of the proteins that manufacture these specific epitopes are also required for virulence of *C. albicans* (36, 43, 44).

These studies have resulted in an understanding of how glycosylation of *C. albicans* proteins influences fungal host-pathogen interaction and virulence. However, little is known regarding the role of glycosylation in the pathogenesis of *C. glabrata*. Simultaneous deletion of the *BMT2–6* genes encoding five

$\beta$ -mannosyltransferases yielded a strain that was unable to induce weight loss or chronic inflammation in a murine colitis model (45). Furthermore, nothing is known regarding the conservation of the glycosylation machinery in this species. We therefore sought to determine the effect of inactivation of three putative components of the *C. glabrata* *N*-linked glycosylation machinery (Anp1, Mnn2, and Mnn11) on cell wall, specifically mannan structure and virulence. We show that there is functional conservation of these enzymes between *C. glabrata* and *S. cerevisiae*. *ANP1* and *MNN11* encode  $\alpha$ -(1–6)-mannosyltransferases, and *MNN2* encodes an  $\alpha$ -(1–2)-mannosyltransferase. Inactivation of each gene results in altered *N*-linked mannan structure consistent with these functions. Furthermore, deletion of the genes differentially affects virulence, and this variability may be partially explained by resultant changes in cellular adhesion.

## EXPERIMENTAL PROCEDURES

**Strains, Media, and Culture Conditions**—All strains used and constructed in this study are listed in Table 1. Fungal cells were routinely cultured in yeast extract peptone dextrose (YPD) (2% (w/v) peptone, 2% (w/v) glucose, 1% (w/v) yeast extract), yeast extract peptone maltose (YPM) (2% (w/v) peptone, 2% (w/v) maltose, 1% (w/v) yeast extract), or synthetic dropout medium (SD) (0.68% (w/v) yeast nitrogen base without amino acids (Difco), 2% (w/v) glucose, and appropriate dropout mix (Clontech) at 30 °C (*S. cerevisiae*) or 37 °C (*C. glabrata*) at 180 rpm. For culture on solid media 2% (w/v), agar was added prior to autoclaving. For phenotypic assays, selective media were made as described by Hampsey (46). Strains were stored at room temperature for up to 4 weeks on solid agar plates or for long term storage in 50% (v/v) glycerol at –80 °C.

**Construction of *C. glabrata* Mutants**—To disrupt *C. glabrata* genes, a one-step PCR-based approach was adopted (47). DNA fragments were amplified using primer pairs such that the PCR product would contain 60 bp of homology to the gene of interest at both the 5' and 3' ends and 20-bp tails homologous to the *C. glabrata* *HIS3* gene, which was amplified from pTW25 (48). Primer sequences are available upon request. The disruption cassette was transformed into *C. glabrata* ΔHT6, and histidine prototrophs were selected on appropriate dropout media. To reconstitute *C. glabrata* genes of interest, the *SAT1* flipper method was used (49). Southern analysis was used to confirm gene disruption at the correct locus and single integration.

## *Candida glabrata* Glycosylation Mutants

The *C. glabrata anp1* null mutant was constructed by removing 1344 bp of the *C. glabrata ANP1* gene (CAGL0L01331g, +1 to +1344 with respect to the start codon, and the stop codon is at +1342) via homologous recombination. Four independent transformants were selected. These strains were all screened in a full phenotypic assay (data not shown), and one mutant was selected for further study, *C. glabrata* XFS-1 (*anp1*). This was made prototrophic by transformation with pCgACT14 (50) to give *C. glabrata* XFS-1P.

To reconstitute *ANP1* in *C. glabrata* XFS-1 plasmids, pLJW6 and pLJW7 were constructed as follows. A NotI-SacII downstream fragment of the *C. glabrata ANP1* gene (positions +1322 to +1772) was amplified from *C. glabrata* 2001 genomic DNA. The resulting 459-bp downstream fragment was digested with NotI and SacII and cloned into NotI-SacII-digested pSFS2 (49) to generate plasmid pLJW6. A KpnI-XhoI fragment containing the complete open reading frame as well as 0.44 kb of upstream and 0.44 kb of downstream flanking sequences of the *ANP1* gene was amplified from *C. glabrata* 2001 genomic DNA. The resulting 2164-bp fragment was digested with KpnI and XhoI and cloned into KpnI-XhoI digested pLJW6 to generate pLJW7. The insert from plasmid pLJW7 was excised as a KpnI-SacII fragment for transformation into *C. glabrata* XFS-1 by electroporation. Cells were spread on YPD plates containing 200  $\mu\text{g}/\text{ml}$  nourseothricin and cultured at 37 °C for 96 h. Four independent transformants were inoculated into YPM liquid medium overnight without nourseothricin to allow for *FLP*-mediated excision of the *SAT1* flipper and nourseothricin-sensitive strains selected on YPD plates containing 10  $\mu\text{g}/\text{ml}$  nourseothricin as detected by their smaller colony size compared with nourseothricin-resistant strains. Southern analysis was used to confirm flipper excision, gene integration at the correct locus, and single integration. Strains were made fully prototrophic by transformation with pCgACT14 and pCgACH3 (50), and then each transformant was subjected to a phenotypic screen (data not shown), and a single strain, *C. glabrata* LJW-5RPL (*anp1::CgANP1*), was selected for further study.

The *C. glabrata mnn2* null mutant was constructed by removing 1839 bp of the *C. glabrata MNN2* gene (CAGL0I04532g, +1 to +1839 with respect to the start codon; the stop codon is at +1837) via homologous recombination. Four independent transformants were selected. These strains were all screened in a full phenotypic assay (data not shown), and one mutant, *C. glabrata* LJW-2 (*mnn2*), was selected for further study. This was made prototrophic by transformation with pCgACT14 to give *C. glabrata* LJW-2P.

To reconstitute *MNN2* in *C. glabrata*, LJW-2 plasmids pLJW8 and pLJW9 were constructed as follows. A NotI-SacII downstream fragment of the *C. glabrata MNN2* gene (positions +1820 to +2250) was amplified from *C. glabrata* 2001 genomic DNA. The resulting 331-bp downstream fragment was digested with NotI and SacII and cloned into NotI-SacII digested pSFS2 to generate plasmid pLJW8. An ApaI-XhoI fragment containing the complete open reading frame as well as 0.44 kb of upstream and 0.30 kb of downstream flanking sequences of the *MNN2* gene were amplified from *C. glabrata* 2001 genomic DNA. The resulting 2583-bp fragment was

digested with ApaI and XhoI and cloned into ApaI-XhoI-digested pLJW8 to generate pLJW9. The insert from plasmid pLJW9 was excised as an ApaI-SacII fragment for transformation into *C. glabrata* LJW-2 by electroporation, and re-integrants were selected, made prototrophic, and confirmed as above to yield *C. glabrata* LJW-2RPL (*mnn2::CgMNN2*).

The *C. glabrata mnn11* null mutant was constructed by removing 1326 bp of the *C. glabrata MNN11* gene (CAGL0G07491g, +1 to +1326 with respect to the start codon, the stop codon is at +1324) via homologous recombination. Four independent transformants were selected. These strains were all screened in a full phenotypic assay (data not shown), and one mutant, *C. glabrata* LJW-3 (*mnn11*), was selected for further study. This was made prototrophic by transformation with pCgACT14 to give *C. glabrata* LJW-3P. *MNN11* was not reconstituted.

**Cross-species Complementation**—To determine whether the functions encoded by the *C. glabrata* and *S. cerevisiae ANP1*, *MNN2*, and *MNN11* orthologues have been conserved, we performed a series of cross-species complementation experiments. First, we sought to determine whether *S. cerevisiae ANP1* could complement phenotypes of the *C. glabrata anp1* mutant. To achieve this, the entire *S. cerevisiae ANP1* open reading frame (−760 to +2480, the stop codon is at +1501) was amplified from *S. cerevisiae* BY4741 (51) genomic DNA. The resulting 3287-bp product was cloned directly into pGEM-T Easy (Promega), excised with BamHI, and cloned into BamHI-digested pCgACT14 to give plasmid pLJW1. pLJW1 was transformed into *C. glabrata* XFS-1 (*anp1*), and tryptophan prototrophs were selected. A representative strain was selected and designated *C. glabrata* LJW-6 (*anp1::ScANP1*).

Next, we sought to determine whether *C. glabrata MNN2* and *MNN11* could complement the phenotypes of the *S. cerevisiae mnn2* and *mnn11* mutants, respectively. To achieve this, the entire *C. glabrata MNN2* (−1265 to +2376, the stop codon is at +1837) and *MNN11* (−1916 to +1911, the stop codon is at +1324) open reading frames plus flanking regions were amplified from *C. glabrata* 2001 genomic DNA. The resulting 3661- and 3779-bp products were cloned directly into pGEM-T Easy, excised with BamHI, and cloned into BamHI-digested YCp111 (52) to give plasmids pLJW3 and pLJW4, respectively. pLJW3 was transformed into *S. cerevisiae mnn2*, and leucine prototrophs were selected. A representative strain was selected and termed *S. cerevisiae* LJW-8 (*mnn2::CgMNN2*). pLJW4 was transformed into *S. cerevisiae mnn11*, and leucine prototrophs were selected. A representative strain was selected and termed *S. cerevisiae* LJW-9 (*mnn11::CgMNN11*).

**Virulence Analysis**—We then sought to determine how inactivation of *ANP1*, *MNN2*, and *MNN11* impacted the ability of *C. glabrata* to cause disease in a well established murine model of systemic candidosis. To achieve this virulence, analysis was performed essentially as described previously (53–55). Briefly, groups of 10–22 out-bred male CD1 mice were immunosuppressed with 200 mg of cyclophosphamide/kg of body weight on day −3 and every 4th day thereafter. Animals were infected with  $7 \times 10^7$  *C. glabrata* yeast cells in 200  $\mu\text{l}$  of saline via tail vein injection. Following infection, mice were weighed and observed daily and sacrificed at predetermined end points, e.g. 20% weight loss.

**Ethics Statement**—All animal work was performed under the auspices of the “Animals (Scientific Procedures) Act 1986” at Imperial College London, United Kingdom. All protocols were approved by the Home Office under project license PPL 70/6487.

**Alcian blue Binding Assay**—Alcian blue binding assays were performed essentially as described previously to determine the extent of mannan phosphorylation (58). Briefly, a suspension of  $1 \times 10^7$  washed exponential phase cells was suspended in 1 ml of 30  $\mu\text{g/ml}$  Alcian blue in 0.02 M HCl (pH 3), incubated at room temperature for 10 min, and pelleted by centrifugation. Then  $A_{600}$  values of 100  $\mu\text{l}$  of supernatant samples were determined in a spectrophotometer. Alcian blue concentration was determined by reference to a standard curve (microgram of Alcian blue bound per  $A_{600}$  unit of cell suspension).

**Mannan Isolation**—To analyze the consequences of gene deletion on mannan structure, mannan was isolated using a modified method first described by Kocourek and Ballou (59). Briefly, 1 liter of saturated culture was collected by centrifugation, and the cells were washed in double distilled water. Washed cells were resuspended in an excess of acetone; the cells were collected by centrifugation, and the supernatant acetone was removed. The cells were dried over Drierite® and under vacuum. The cells were rehydrated in 200 ml of double distilled water and subjected to autoclaving for 3 h, and after cooling the solid extract was collected by centrifugation and the remaining supernatant subjected to Fehling precipitation. An equal volume of Fehling’s solution (50:50 Fehling’s Solution No. 1 and No. 2) was added to the extracted mannan mixture with stirring, and a precipitate of copper-mannan was then formed and allowed to settle. The remaining supernatant was removed, and the copper complex was dissolved in 6 ml of 3 M HCl. The resulting solution was poured slowly, with stirring, into a 100-ml (8:1) mixture of methanol/acetic acid, and the resulting precipitate was allowed to settle overnight. The supernatant was decanted, and the precipitate was stirred with a fresh methanol/acetic acid mixture to remove the copper complex. This was repeated until the solution appeared colorless. The precipitate was collected and washed several times with methanol and allowed to dry under vacuum.

**Proton and Carbon-13 NMR**—Structural analysis of the mannan extracts was performed using one- and two-dimensional proton (60) and carbon-13 NMR (61). NMR spectra were collected on a JEOL Eclipse+ 600 NMR spectrometer operating at  $80 \pm 1^\circ\text{C}$  in 5-mm NMR tubes. Mannan was dissolved in  $\text{D}_2\text{O}$  at  $80 \pm 1^\circ\text{C}$ . Proton chemical shifts were referenced to sodium 3-trimethylsilylpropionate-2,2,3,3- $d_4$ . C-13 chemical shifts were referenced to external acetone. Proton one-dimensional NMR spectral collection and processing parameters were as follows: 25 ppm spectral width centered at 7.5 ppm, 32,768 data points, 1024 scans, 15 s relaxation delay, 2.18 s acquisition time, and exponential apodization. C-13 one-dimensional NMR spectral collection and processing parameters were as follows: 250 ppm spectral width centered at 110 ppm, 65,536 data points, 3161 scans, 5 s relaxation delay, 1.74 s acquisition time, and exponential apodization. Homonuclear gradient COSY two-dimensional NMR spectra were collected and processed as follows:  $512 \times 128$  point matrix was zero-filled to

$512 \times 1024$  points, 256 scans per row with 4 dummy scans, 3 ppm sweep width centered at 4.5 ppm, sinebell apodization in both dimensions, and 1 s relaxation delay. NMR spectra were processed using JEOL DELTA software running on the Eclipse+ 600 NMR and on a Macintosh MacBook Pro.

**Gel Permeation Chromatography-Multiangle Laser Light Scattering (GPC/MALLS)<sup>3</sup> Detection**—Further structural analysis was performed by high performance GPC/MALLS photometry as reported previously by Müller *et al.* (62) and Adams *et al.* (63) to determine the polysaccharide weight averaged molecular mass and root mean square (r.m.s.) radius. Briefly, the mannan samples were dissolved at 3 mg/ml, heated for 15 min at  $60^\circ\text{C}$ , cooled, and filter-sterilized in 50 mM sodium nitrite mobile phase. Three Ultrahydrogel columns (1200, 500, and 100; Waters) were connected in a series, and the columns were maintained at  $37 \pm 1^\circ\text{C}$  with continuous mobile phase flow. The system was calibrated using narrow band pullulan standards (Showa Denko, Japan). The weight-average molecular mass and the  $z$  average radius of the center of gravity as an index of molecular size of the samples were determined by on-line MALLS photometry employing a Wyatt Technology TriStar MALLS ( $\lambda = 690$  nm) photometer. Data were acquired and analyzed using Astra software (version 4.9; Wyatt Technology).

**Flow Adhesion Assay of C. glabrata Mutants**—To determine whether gene deletion affected cellular adherence, we used a well established endothelial flow assay performed essentially as described previously (64). Briefly, *C. glabrata* was cultured overnight in liquid YPD at  $37^\circ\text{C}$ , 180 rpm, washed three times with sterile Hanks’ buffered salt solution (Invitrogen), counted, and resuspended at  $1.0 \times 10^6$  yeast/ml in Hanks’ buffered salt solution. Glass slides coated with confluent HMEC-1 endothelial cell monolayers were mounted in a parallel plate flow chamber (GlycoTech, Rockville, MD), and *C. glabrata* cells were perfused through the flow chamber and over the endothelial cell monolayer, using an automated syringe pump at 0.25 dynes/cm<sup>2</sup> (Harvard Apparatus, Natick, MA). All experiments were performed on a  $37^\circ\text{C}$  stage, in an environmental microscope chamber also maintained at  $37^\circ\text{C}$ . Adhesion events were visualized using a Zeiss Axiovert 200 M inverted fluorescence microscope. An integrated high resolution AxioCam digital camera (Nikon) with Axiovision 4.6 software (Imaging Associates Ltd., Bicester, UK) was used to record the flow experiments. *C. glabrata* suspensions were allowed to perfuse the flow chamber for 2 min before commencing recording. Results consisted of 15-min recordings of a random field of view (0.15 mm<sup>2</sup>) using a  $\times 20$  objective. Each experiment was repeated with three separate confluent endothelial cell slides on at least two occasions. Cell motion analysis was performed using time-lapse software. Images were then acquired over 15 min into a video file at 2 frames/min, and the total number of adherent cells/mm<sup>2</sup> was recorded.

<sup>3</sup> The abbreviations used are: GPC/MALLS, gel permeation chromatography-multiangle laser light scattering; r.m.s., root mean square.

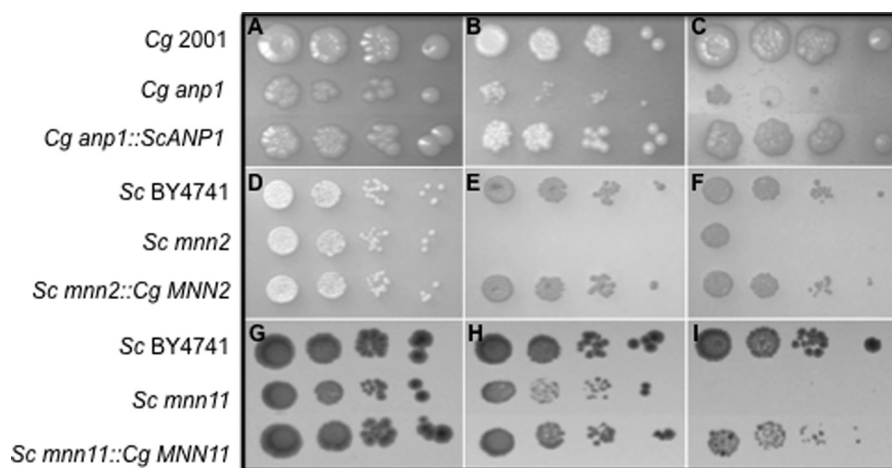


FIGURE 1. *C. glabrata* 2001 *ANP1*, *MNN2*, and *MNN11* encode functional homologues of *S. cerevisiae* *Anp1*, *Mnn2*, and *Mnn11*. A–I, 10-fold serial dilution of yeast strains were cultured on YPD (A, D, and G); YPD plus 10 mM caffeine (B); YPD plus 1 mg/ml Calcofluor White (C and F); YPD plus 50  $\mu$ g/ml hygromycin (I), or YPD plus 3 mM sodium orthovanadate (E and H) at 37 °C (A–C) or 30 °C (D–I) for 48 h. *S. cerevisiae* *ANP1* complements the growth defects of *C. glabrata anp1* cells on caffeine (B) and Calcofluor White (C). Similarly, *C. glabrata* *MNN2* and *MNN11* complement the growth defects of *S. cerevisiae* *mnn2* and *mnn11* cells, respectively on sodium orthovanadate (E and H); Calcofluor White (F), and hygromycin (I). This demonstrates that *C. glabrata* and *S. cerevisiae* *ANP1*, *MNN2* and *MNN11* encode at least partial functional homologues.

## RESULTS

*ANP1*, *MNN2*, and *MNN11* Gene Functions Are Conserved between *C. glabrata* and *S. cerevisiae*—To determine whether *C. glabrata* *ANP1*, *MNN2*, and *MNN11* encode functional homologues of the *S. cerevisiae*  $\alpha$ -(1–6)-mannosyltransferases (*Anp1* and *Mnn11*) and  $\alpha$ -(1–2)-mannosyltransferase (*Mnn2*), we conducted a series of cross-complementation experiments. *S. cerevisiae* *ANP1* was able to successfully rescue the caffeine, SDS, Calcofluor White, hygromycin B, and NaCl sensitivities of the *C. glabrata anp1* null mutant (Fig. 1, A–C, and data not shown). Similarly *C. glabrata* *MNN2* and *MNN11* were able to rescue phenotypes associated with *S. cerevisiae* *mnn2* and *mnn11* null mutants, respectively (Fig. 1, D–I, and data not shown). This demonstrates that the genes in the two species encode at least partial functional homologues.

In addition to these complementation studies, we determined the consequences of the individual *C. glabrata* gene deletions to various perturbations. As anticipated, all three mutants had phenotypes consistent with a weakened cell wall. The *C. glabrata anp1* null mutant was hypersensitive to the cell wall perturbing agents Calcofluor White and SDS and the stress-inducing agent NaCl. Furthermore, analogous to glycosylation-defective strains in *S. cerevisiae*, the *C. glabrata anp1* null mutant was hypersensitive to hygromycin B (Fig. 2, A–C, data not shown). Comparatively, *C. glabrata mnn2* was unaffected for growth on hygromycin B, NaCl, and SDS but harbored a cell wall defect of sorts as the null mutant was hypersensitive to Calcofluor White and sodium orthovanadate (Fig. 2, D–F, data not shown). *C. glabrata mnn11* was hypersensitive to Calcofluor White, NaCl, hygromycin B, sodium orthovanadate, and to growth at 42 °C (Fig. 2, G–I). In liquid culture, all three null mutants exhibited slight growth defects with doubling times of 54 min (*mnn11*), 60 min (*mnn2*), and 70 min (*anp1*) in YPD at 37 °C compared with 45 min for *C. glabrata* 2001. In addition, *C. glabrata mnn2* and *mnn11* tended to form small cellular aggregates that could be largely dispersed by vigorous vortexing. These data strongly support the hypothesis

that *C. glabrata* *Anp1*, *Mnn2*, and *Mnn11*, as expected for mannosyltransferases, play roles, as do their counterparts in *S. cerevisiae*, in maintaining cell wall integrity.

*Structure of C. glabrata* Mannan—Our cross-complementation experiments strongly suggest that *C. glabrata* *ANP1*, *MNN2*, and *MNN11* encode functional homologues of the respective *S. cerevisiae* mannosyltransferases. Hence, we would anticipate that their inactivation should result in changes to mannan structure, specifically that the *anp1* and *mnn11* mutants would have shorter  $\alpha$ -(1–6)-polymannosyl backbones, as they would have reduced  $\alpha$ -(1–6)-mannosyltransferase activity, and the *mnn2* null would lack  $\alpha$ -(1–2)-mannose side chains, due to loss of  $\alpha$ -(1–2)-mannosyltransferase. To verify this, we carried out a series of physicochemical and structural analyses.

Initially, GPC/MALLS was used to compare the molecular weight and r.m.s. radii of mannans from *C. glabrata* 2001, *anp1*, *mnn2*, and *mnn11* strains. Pullulan was used as a control. The mannans from all three mutants showed polymer distributions that were different from *C. glabrata* 2001. Specifically, mannans from the mutants were characterized by a larger quantity of lower molecular weight polymers (Fig. 3A and Table 2). For example, the polymer distribution of *C. glabrata mnn2* mannan is clearly shifted downfield in the GPC/MALLS chromatogram (Fig. 3B) which is indicative of a lower molecular weight mannan compared with the wild-type *C. glabrata* 2001 strain. This was also the case for mannans from *anp1* and *mnn11* cells, as would be expected if the mannan polymers had a lower degree of polymerization as a result of a shorter  $\alpha$ -(1–6) backbone or missing  $\alpha$ -(1–2) side chains. The r.m.s. radius provides an indication of the volume that the molecules occupy in three-dimensional space. *C. glabrata mnn2* mannan has a 47.4% reduction in r.m.s. radius compared with *C. glabrata* 2001, suggesting that it contains the fewest mannose monosaccharides of all strains tested. Reductions of 29.2 and 29.9% were observed in the *anp1* and *mnn11* mannans (Table 2).

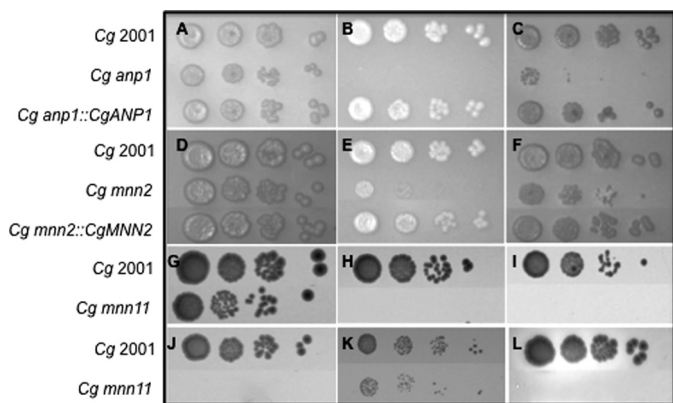


**FIGURE 2. *C. glabrata anp1* and *mnn2* cells exhibit phenotypes associated with weakened cell walls.** A–L, 10-fold serial dilution of yeast strains were cultured on YPD (A, D, and G); YPD plus 1 mg/ml Calcofluor White (B, E, and I); YPD plus 50  $\mu$ g/ml hygromycin (C, F and J); YPD plus 3 mM sodium orthovanadate (H); YPD plus 1.5 M NaCl at 37 °C for 48 h (K), or YPD at 42 °C for 48 h (L). *C. glabrata anp1* (A–C) and *mnn2* mutants (D–F) exhibit reduced growth, compared with wild-type *C. glabrata* cells, on Calcofluor White (B and E) and hygromycin (C and F). Reintegration of *C. glabrata ANP1* (A–C) or *MNN2* (D–F) into the appropriate mutant background restored wild-type growth characteristics. H–L, *C. glabrata mnn11* mutants exhibit reduced growth, compared with wild-type *C. glabrata* cells, at 42 °C (H) and in the presence of sodium orthovanadate (I), hygromycin (J), NaCl (K), and Calcofluor White (L).

To further characterize these differences we performed  $^1\text{H}$  NMR studies. Chemical shift assignments for the anomeric proton, H1, and H2 of the mannosyl repeat units in the backbone and side chain structural fragments were obtained from COSY spectra (data not shown). These studies show (Table 3) that *C. glabrata* 2001, *anp1*, and *mnn11* mannans (Fig. 4, A–C, respectively) are distinctly different from the mannan isolated from *C. glabrata mnn2* (Fig. 4D). Specifically, the *C. glabrata* 2001, *anp1*, and *mnn11* mannans exhibit resonances that are assigned to structural fragments in  $\alpha$ -(1,2)-linked (60) and possibly  $\alpha$ -(1,3)-linked (65) mannosyl repeat units in side chains attached to the  $\alpha$ -(1,6)-linked backbone chain with all backbone repeat units containing side chains (Table 3). Also, the presence of mannosyl repeat units associated with the phosphodiester linkage between acid-stable and acid-labile portions of the mannan structure is evident for 2001, *anp1*, and *mnn11*. In addition, the proton NMR spectrum of *mnn11* mannan (Fig. 4C) indicates a reduced level of  $\text{M}\beta\text{1}-2\text{M}\alpha\text{1}$ , side chains compared with 2001 and *anp1* mannans based on the reduced intensity of the resonances near 4.78 and 5.18 ppm (Fig. 4C, indicated by vertical arrows). These resonances are assigned to the anomeric protons of the  $\text{M}\beta\text{1}$ - and  $-2\text{M}\alpha\text{1}$  structural fragments, respectively, of the  $\text{M}\beta\text{1}-2\text{M}\alpha\text{1}$  side chain structural fragment. The predominant resonances for *C. glabrata mnn2* mannan support the presence of backbone mannosyl repeat units without attached side chains based upon the major anomeric proton resonance at 4.91 ppm. This singlet resonance at 4.91 ppm is assigned to an anomeric proton of the  $\alpha$ -(1,6)-linked backbone mannosyl repeat unit ( $-\text{M}\alpha\text{1}-6\text{M}\alpha\text{1}-6\text{M}\alpha-$ ) containing no side chains (66, 67). Also, significant side chain structural fragments containing  $\alpha$ -(1,2)-linked and possibly  $\alpha$ -(1,3)-linked mannosyl repeat units (60, 65) are not indicated based upon the reduced level of these resonances in the 5.0–5.3 ppm spectral region. The side chains in the *mnn2* mannan are considerably shorter than in 2001, *anp1*, and *mnn11* mannans.

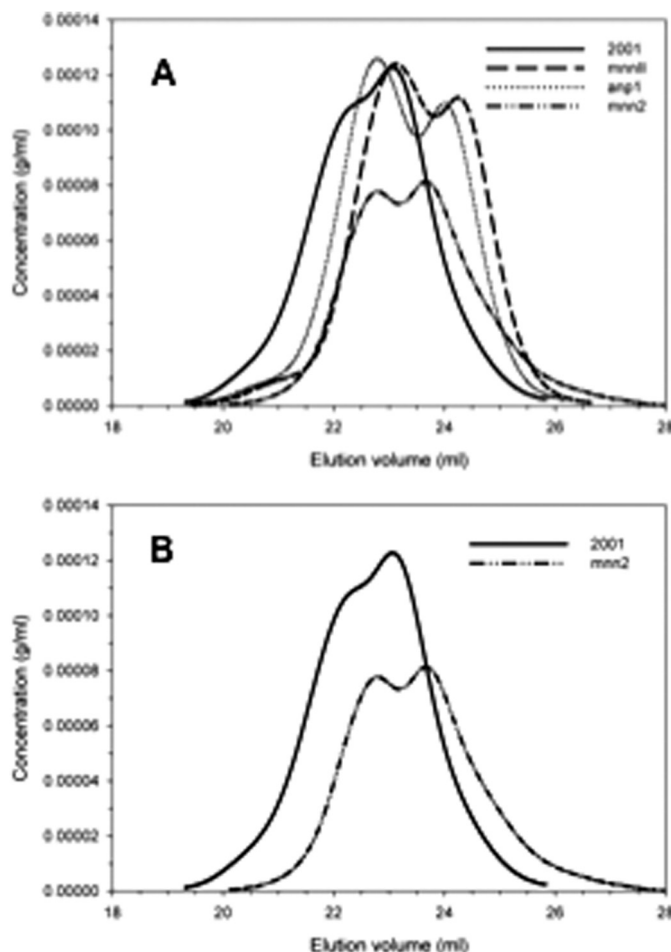


**FIGURE 3. Molecular weights of *C. glabrata anp1*, *mnn2*, and *mnn11* mannans are lower than mannan isolated from wild-type cells.** A, refractive index (concentration) chromatogram of *C. glabrata anp1* (dotted line), *mnn2* (hashed and dotted line), and *mnn11* (hashed line) mannans are shifted downfield indicating a lower molecular weight than mannan isolated from wild-type (solid line) cells. B, this is particularly evident in the downfield shift for the *mnn2* mannan (hashed and dotted line) when compared with wild-type mannan (solid line). The average molecular weight, polydispersity, and r.m.s. radii for all four mannans and a pullulan standard are shown in detail in Table 2. All mannan samples were passed through three Ultrahydrogel columns (1200, 500, and 100, Waters) connected in series, and the weight-average molecular mass, polydispersity, and r.m.s. radius of the samples were determined by on-line MALLS photometry as described under "Experimental Procedures."

**TABLE 2**  
Comparison of molecular weight and rms radii for mannans isolated from *C. glabrata* 2001, *anp1*, *mnn2* and *mnn11*

Strain	Molecular weight <sup>a</sup>	r.m.s. radius <sup>b</sup>
	g/mol	nm
Pullulan <sup>c</sup>	$1.10 \times 10^5$	25.4
2001	$1.54 \times 10^5$	25.4
<i>anp1</i>	$1.09 \times 10^5$	22.1
<i>mnn2</i>	$0.81 \times 10^5$	26.1
<i>mnn11</i>	$1.08 \times 10^5$	23.6

<sup>a</sup> Molecular weight is expressed as weight average molecular weight in g/mol. It is representative of the average molecular weight over the entire polymer distribution.

<sup>b</sup> The r.m.s. radius is a measure of a polymer's size weighted by the mass distribution about its centre of mass.

<sup>c</sup> Pullulan (Showa Denko, Japan) was used as a standard.

Predominant side chain structure arises from side chains containing single  $\alpha$ -(1,2)- or  $\alpha$ -(1,3)-linked mannosyl repeat units or short chains containing single  $\alpha$ -(1,2)- or  $\alpha$ -(1,3)-linked mannosyl repeat units terminated by 1–3  $\beta$ -(1,2)-linked man-

**TABLE 3**

Significant mannanyl structural fragments present in the mannans purified from *C. glabrata* 2001, *anp1*, *mnn2*, and *mnn11*

Structural fragments <sup>a</sup>	2001	<i>anp1</i>	<i>mnn11</i>	<i>mnn2</i>
→2Mα1→PO <sub>4</sub>	Yes	Yes	Yes	No
α1→2Mα1→2	Yes	Yes	Yes	Yes
Mβ1-2Mα1-2(3) <sup>b</sup>	Yes	Yes	Minor	No
Mα1→2(3)	Yes	Yes	Yes	Yes
Mα1→3	Yes	Yes	Yes	Yes
1→6M(→2)1→6M(→2)Mα1α1→6M(→2)1→	Yes	Yes	Yes	Yes
1→6M(→2)1→6M(→2)Mα1→2Mα1α1→6M(→2)1→	Yes	Yes	Yes	No
α1→3Mα1→2	Yes	Yes	Yes	No
→6M(→2)Mα1α1→6M(→2)Mα1→2α1→6	No	No	No	Yes
α1→2Mα1→2	No	No	No	Yes
α1→6Mα1→6	No	No	No	Yes
Mβ1(→2Mβ1) <sub>n</sub> →2Mα1→(2(3) or PO <sub>4</sub> ) [ <i>n</i> = 1 or 2]	Yes	Yes	Yes	Yes
Mβ1→2Mα1→PO <sub>4</sub>	Yes	Yes	Yes	No
Mβ1→2Mα1→2	Yes	Yes	Minor	No
Mβ1→2Mα1→	No	No	No	Yes

<sup>a</sup> Structural fragment identifications are based upon analysis of COSY two-dimensional NMR spectra observed for each isolate. In each fragment, "M" refers to the mannanyl repeat unit. The number represents the point of attachment within the specified mannanyl repeat unit. Proton numbering is indicated in the monomer structure shown in Fig. 4. α and β indicate the conformation at the anomeric carbon.

<sup>b</sup> "2(3)" indicates that the point of attachment to the neighboring mannanyl repeat unit could be either at the 2- or 3-position.

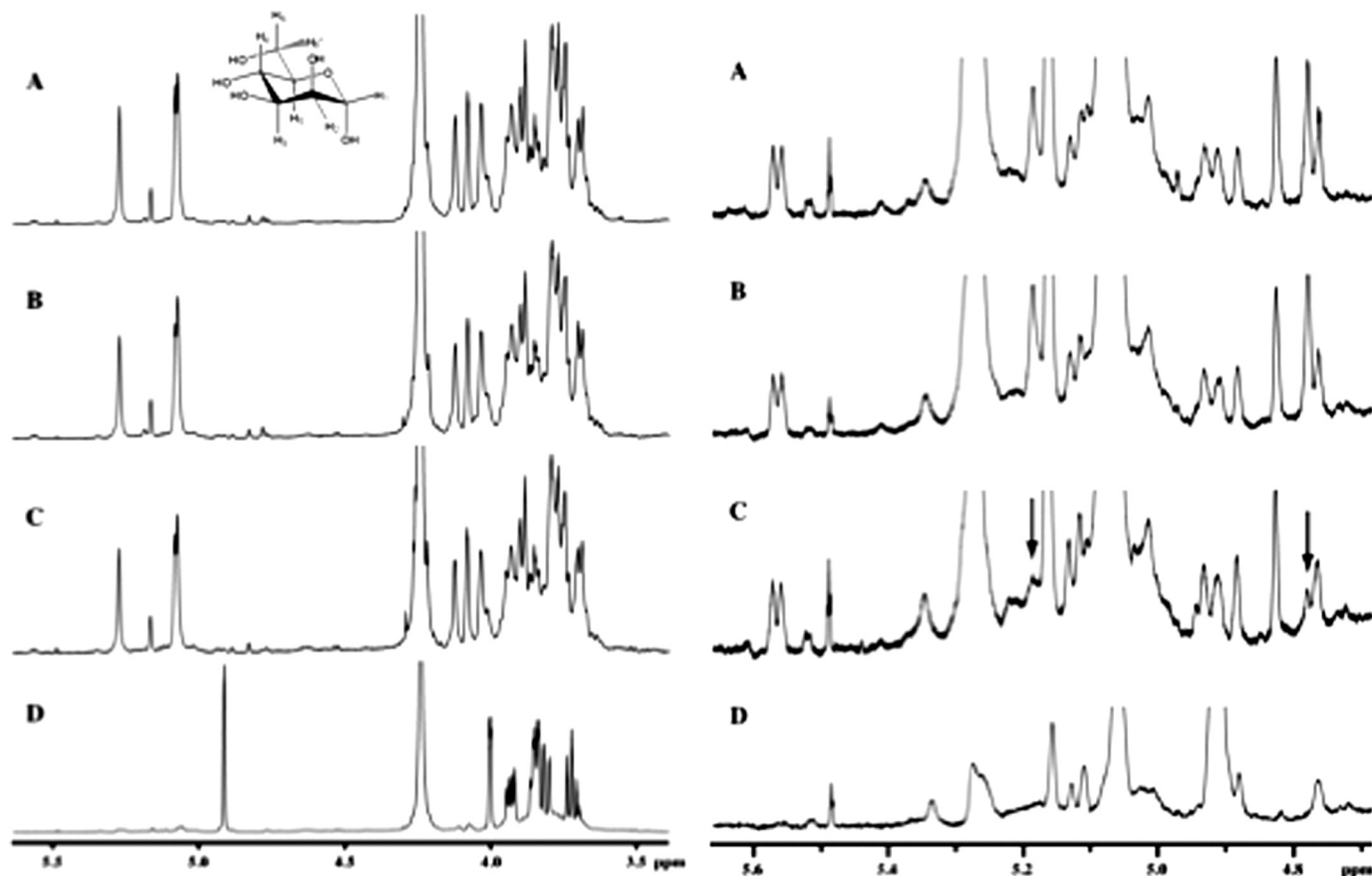


**FIGURE 4.** *C. glabrata mnn2* mannan is distinct from other mannans analyzed and lacks α-(1,2)-linked mannans side chains, whereas *mnn11* mannan is similar to 2001 and *anp1* mannans but contains a reduced level of Mβ1-2Mα1 side chains. Comparison of mannans <sup>1</sup>H NMR spectra for *C. glabrata* 2001 (A), *anp1* (B), *mnn11* (C), and *mnn2* (D). The carbohydrate spectral regions for all four mannans plotted from 3.4 to 5.6 ppm are compared on the left, and the expanded anomeric proton spectral regions for all four mannans plotted from 4.7 to 5.65 ppm are compared on the right. The mannan from *C. glabrata mnn2* is distinctly different from the other mannans because it lacks resonances in the 5.0–5.3 ppm spectral region for α-(1,2)-linked mannans side chain repeat units. The mannan from *mnn11* is similar to but slightly different compared with mannans from 2001 and *anp1* due to the reduced level of Mβ1-2Mα1 end groups indicated by the smaller resonances near 4.78 and 5.18 ppm (indicated by vertical arrows). Proton NMR spectra were collected on a JEOL Eclipse+ 600 NMR spectrometer operating at 80 ± 1 °C in 5-mm NMR tubes. Each mannan isolate was dissolved in D<sub>2</sub>O at 80 °C ± 1 °C. Proton chemical shifts were referenced to sodium 3-trimethylsilylpropionate-2,2,3,3-*d*<sub>4</sub>.

nosyl repeat units. In addition, only the acid-stable portion of the mannan structure is observed in the *mnn2* mannan because anomeric protons associated with acid-labile mannans repeat units in side chains attached to a phosphodiester linkage are not evident (Table 3). <sup>13</sup>C NMR (Fig. 5) with six resonances whose chemical shifts compare favorably with an α-(1,6)-mannan dimer model compound (61) confirms this structural assignment. Proton and <sup>13</sup>C NMR chemical shift assignments along with structural fragment and dimer chemical shifts for *C. glabrata mnn2* mannan are summarized in Table 4. Therefore, *C. glabrata mnn2* expresses nearly pure α-(1,6)-mannan with fewer or shorter side chains, whereas *C. glabrata* 2001, *anp1*, and *mnn11* express mannan containing side chains (Table 3).

The Alcian blue assay showed that inactivation of *MNN2* resulted in a 75% reduction in mannans phosphorylation compared with wild-type cells, whereas the relative reduction was only 50% when *ANP1* or *MNN11* was deleted (Fig. 6). Furthermore, the *C. glabrata* 2001 <sup>1</sup>H NMR spectrum shows a doublet resonance at 5.57 ppm from phosphorylation of the mannan (Fig. 4B), which the *C. glabrata mnn2* spectrum lacks (Fig. 4D). This supports the data from the Alcian blue experiments of decreased mannans phosphorylation in the *mnn2* null mutant,



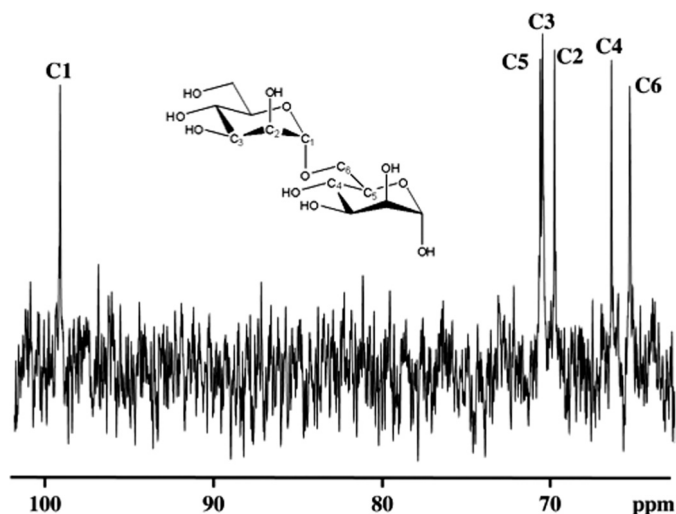


FIGURE 5. *C. glabrata mnn2* cell wall contains  $\alpha$ -(1,6)-mannan. The  $^{13}\text{C}$  NMR spectrum of  $\alpha$ -(1,6)-mannan extracted from *C. glabrata mnn2* cells is shown. Resonance chemical shifts are assigned to specific carbons in Table 4. Resonances are labeled and assigned based on the  $\alpha$ -(1,6)-linked mannan dimer shown (61).

TABLE 4

*C. glabrata mnn2* mannan  $^1\text{H}$  and  $^{13}\text{C}$  NMR chemical shifts

*C. glabrata mnn2* mannan  $^1\text{H}$  and  $^{13}\text{C}$  NMR chemical shifts (in ppm) are compared with the reference assignments for protons, and an  $\alpha$ -(1,6)-mannan dimer (61) for  $^{13}\text{C}$ . Proton labels are shown in the mannose monomer structure in Fig. 4. The structure of the dimer with carbon labels is shown in Fig. 5. Proton and  $^{13}\text{C}$  NMR spectra were collected on a JEOL Eclipse+ 600 NMR spectrometer operating at  $80^\circ\text{C} \pm 1^\circ\text{C}$  in 5-mm NMR tubes. Mannan was dissolved in  $\text{D}_2\text{O}$  at  $80^\circ\text{C} \pm 1^\circ\text{C}$ . Proton chemical shifts were referenced to sodium 3-trimethylsilylpropionate-2,2,3,3- $d_4$ .  $^{13}\text{C}$ -13 chemical shifts were referenced to external acetone.

Nucleus	$^1\text{H}$ NMR		$^{13}\text{C}$ NMR	
	This work	Reference assignment	This work	Dimer (61)
1	4.911	4.920 (66) 4.918 (60)	99.38	100.3
2	4.002	4.009 (66) 4.011 (60)	70.02	70.8
3	3.854	3.856 (60)	70.72	71.5
4	3.736		66.64	67.4
5	3.854		70.86	71.6
6	3.943		65.56	66.5
6'	3.812			

and it suggests that the  $\alpha$ -(1,2)-mannose side branches are important sites for mannosyl phosphate linkage.

Taken together, these data strongly support the view that Anp1, Mnn2, and Mnn11 function as mannosyltransferases in *C. glabrata*, and both *S. cerevisiae* and *C. glabrata* mannans are structurally similar but distinct from *C. albicans* mannan (65).

**Role of *C. glabrata* Anp1, Mnn2, and Mnn11 in Virulence**—Having determined that *C. glabrata* ANP1, MNN2, and MNN11 encode functional homologues of the orthologous *S. cerevisiae* proteins, we sought to investigate their role in virulence. To achieve this, we used an established murine model of systemic infection (53–56). Groups of neutropenic male CD1 mice were inoculated with  $7 \times 10^7$  *C. glabrata* cells and were followed as described under “Experimental Procedures.”

The *C. glabrata anp1* null was significantly increased in virulence with 100% mortality by day 5, compared with 20% survival over 14 days for the wild-type control (Fig. 7A, Kaplan-Meier log rank test;  $p < 0.01$ ). Reconstitution of ANP1 restored the phenotype to wild-type levels with 20% survival over 14 days

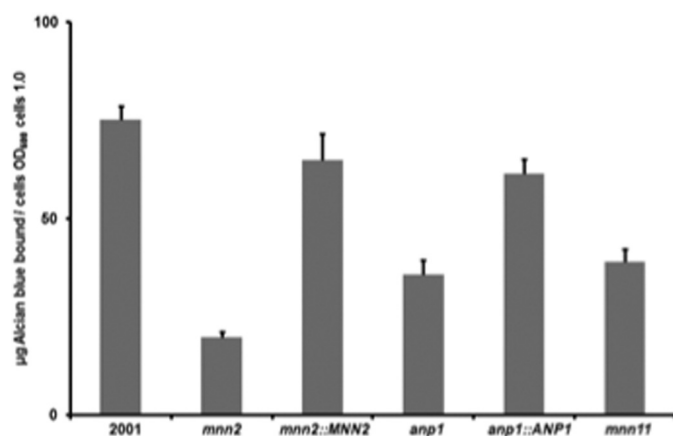


FIGURE 6. *C. glabrata anp1*, *mnn2*, and *mnn11* cells are deficient in mannosyl phosphorylation. Binding of Alcian blue to *C. glabrata* 2001, *anp1*, *anp1::ANP1*, *mnn2*, *mnn2::MNN2*, and *mnn11* cells. *C. glabrata anp1*, *mnn2*, and *mnn11* cells show statistically significant reduced levels of Alcian blue binding compared with wild-type cells ( $p < 0.05$ ,  $t$  test). Reintegration of *MNN2* to the appropriate null mutant restored the capacity to bind Alcian blue ( $p > 0.05$ ,  $t$  test), and reintegration of *ANP1* partially restored Alcian blue binding capacity. Results (mean  $\pm$  S.D.) are pooled triplicate data from a representative experiment. Exponentially growing *C. glabrata* cells were suspended in Alcian blue, incubated at room temperature for 10 min, and pelleted by centrifugation. Then,  $A_{600}$  values of 100  $\mu\text{l}$  supernatant samples were determined in a spectrophotometer, and Alcian blue concentration was determined by reference to a standard curve.

( $p > 0.05$ ). Therefore, inactivation of *C. glabrata anp1* results in a hypervirulent phenotype in our mouse model. Similarly, the *C. glabrata mnn2* null was significantly increased in virulence with 100% mortality by day 4, compared with 20% survival over 14 days for the wild-type control (Fig. 7B,  $p < 0.0001$ ). Reconstitution of *MNN2* restored virulence to wild-type levels with 20% survival over 14 days ( $p > 0.05$ ). Therefore, inactivation of *C. glabrata mnn2* results in a hypervirulent phenotype in our mouse model.

In contrast, the *C. glabrata mnn11* null was unaffected in virulence with 40% survival by day 14, compared with 20% survival over 14 days for the wild-type control (Fig. 7C,  $p > 0.5$ ). No *MNN11* reconstitution experiments were performed as virulence was wild type in the *mnn11* null. Hence, deletion of *MNN11* has no effect on virulence in our mouse model.

***C. glabrata mnn2* Cells Are Hyperadherent to Endothelial Cells**—To determine whether the structural differences in the cell wall were able to affect the adherence capacity of the strains, and hence at least partially explain the differences in virulence observed, we employed a flow adhesion assay. *C. glabrata* cells were perfused through a flow chamber over a confluent layer of HMEC-1 endothelial cells for 15 min. Adhered cells were scored at 0, 5, 10, and 15 min for each strain, and the results from a representative experiment (three technical replicates) are shown in Fig. 8. *C. glabrata* adhesion to the endothelial cells was extremely rapid with adhesion noted for all strains after 5 min. *C. glabrata mnn2* was hyperadherent compared with *C. glabrata* 2001, with statistically increased levels of adhesion at all time points (5 and 10 min,  $p < 0.05$ ; 15 min,  $p < 0.001$ ;  $t$  test). *C. glabrata anp1* also showed statistically significantly increased adherence compared with *C. glabrata* 2001 at 15 min ( $p < 0.05$ ,  $t$  test), although the increase was modest. *C. glabrata mnn11* was statistically unaffected in

## Candida glabrata Glycosylation Mutants

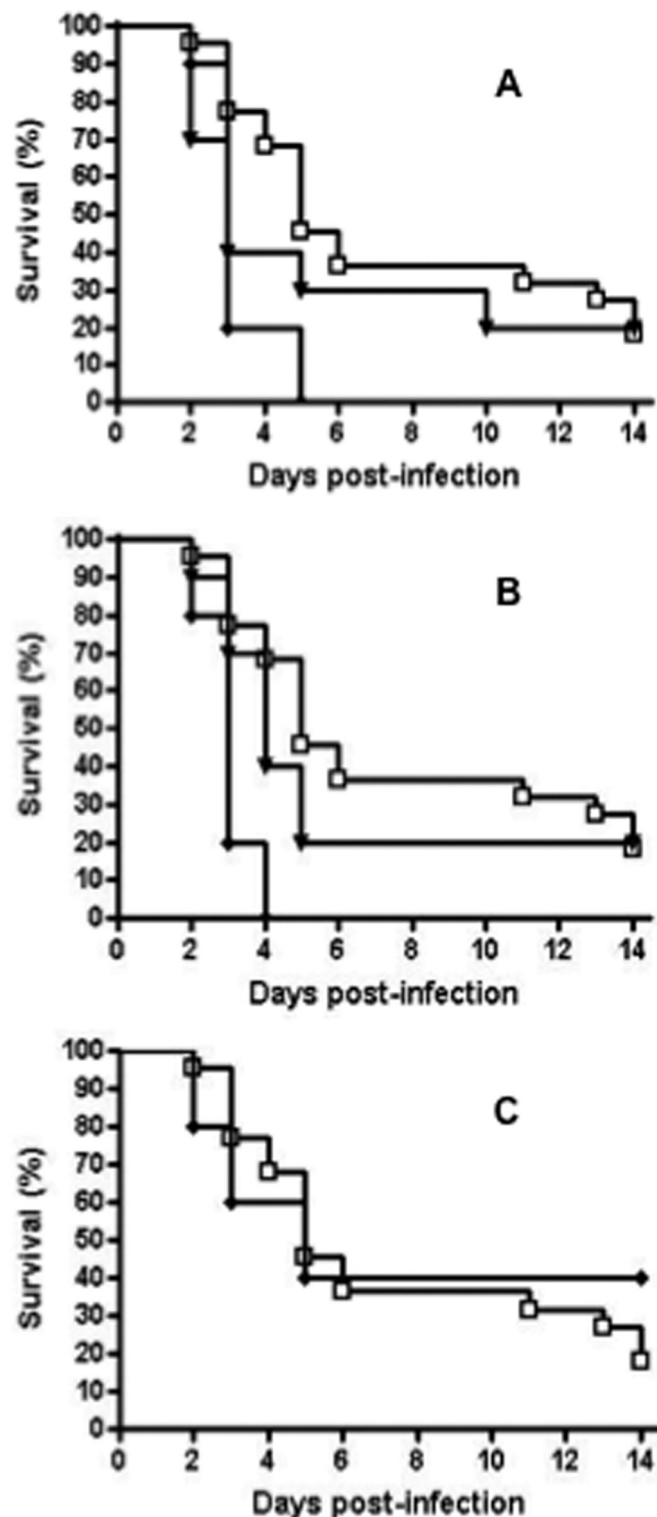


FIGURE 7. *C. glabrata anp1* and *mnn2* are hypervirulent. A, survival curves for mice infected with *C. glabrata* 2001 (open squares), *anp1* (closed diamond), and *anp1::ANP1* (closed triangles). Intravenous infection with the *C. glabrata anp1* null mutant at  $7 \times 10^7$  cells/mouse resulted in a hypervirulent phenotype with 100% mortality within 5 days, compared with the wild-type strain at the same dose resulting in 20% survival over 14 days. This result is significant ( $p < 0.01$ , Kaplan-Meier log rank analysis). The reintegrant control restored virulence to wild-type levels with 20% survival over 14 days ( $p > 0.05$ , Kaplan-Meier log rank analysis). B, survival curves for mice infected with *C. glabrata* 2001 (open squares), *mnn2* (closed diamond), and *mnn2::MNN2* (closed triangles). Intravenous infection with the *C. glabrata mnn2* null mutant at  $7 \times 10^7$  cells/mouse resulted in a hypervirulent phenotype with 100% mortality

adherence compared with *C. glabrata* 2001 for all measured time points. Hence, both the *C. glabrata mnn2* and *anp1* endothelial cell interactions were altered as characterized by a hyperadherent phenotype *in vitro*, albeit modest in the case of *C. glabrata anp1* cells.

### DISCUSSION

Complementation analyses showed that the *C. glabrata ANP1*, *MNN2*, and *MNN11* encode functional homologues of the respective *S. cerevisiae* proteins. Therefore, we predict that both *C. glabrata Anp1* and *Mnn11* are  $\alpha$ -(1,6)-mannosyltransferases, whereas *Mnn2* functions as an  $\alpha$ -(1,2)-mannosyltransferase (26). As anticipated, inactivation of each gene resulted in phenotypic consequences suggestive of changes in cell wall structure and integrity.

To investigate the structural basis for these phenotypic changes, we compared the mannans in each mutant to wild-type *C. glabrata*. All three mutants had mannans that exhibited lower molecular weight than mannan isolated from wild-type cells. The 48% reduction in molecular weight of *C. glabrata mnn2* demonstrates that this mannan contains the fewest mannosyl repeat units of all strains tested, which we suggest is due to an inability of the mutant to catalyze the addition of  $\alpha$ -(1-2)-mannose residues to the  $\alpha$ -(1-6)-linked mannosyl backbone resulting in long unbranched mannans. This is in agreement with a lack of  $\alpha$ -(1-2)-mannose residues seen in an *S. cerevisiae mnn2* strain (68). In contrast, the *C. glabrata anp1* and *mnn11* strains display a less dramatic decrease in their molecular weight (degree of polymerization). Although their mannan backbone chains are shorter,  $\alpha$ -(1-2)-mannose residues can still attach. Thus, the overall molecular weight of the *anp1* and *mnn11* mannan polymers is higher than that observed for *C. glabrata mnn2* mannan.

The Alcian blue assay showed that inactivation of *MNN2* resulted in a 75% reduction in mannosyl phosphorylation compared with wild-type cells, whereas the relative reduction was only 50% when *ANP1* or *MNN11* was deleted. The mannosyl phosphorylation that was observed is likely due to attachment of phosphomannan to either the *N*-linked core structure or *O*-mannan. However, the lower level of mannosyl phosphorylation in *C. glabrata mnn2* cells indicates that the  $\alpha$ -(1,2)-mannose side chains harbor mannosyl phosphorylation linkage points, as seen in *S. cerevisiae N*-glycans (69) and similar to what has been reported in *C. glabrata N*-glycan structural studies (17, 18). The  $^1\text{H}$  NMR spectrum of mannan extracted from

within 4 days, compared with the wild-type strain at the same dose resulting in 20% survival over 14 days. This result is significant ( $p < 0.0001$ , Kaplan-Meier log rank analysis). The reintegrant control restored virulence to wild-type levels with 20% survival over 14 days ( $p > 0.05$ , Kaplan-Meier log rank analysis). C, survival curves for mice infected with *C. glabrata* 2001 (open squares) and *mnn11* (closed diamond). Intravenous infection with the *C. glabrata mnn11* null mutant at  $7 \times 10^7$  cells/mouse resulted in a wild-type phenotype with 40% survival over 14 days, compared with the wild-type strain at the same dose with 20% survival over 14 days. This result is not significant ( $p > 0.5$ , Kaplan-Meier log rank analysis). Groups ( $n = 22$  wild-type cells;  $n = 10$  for all mutants) of outbred CD1 mice were immunosuppressed with cyclophosphamide and infected with  $7 \times 10^7$  *C. glabrata* yeast cells via tail vein injection. Following infection, mice were weighed and observed daily and sacrificed at predetermined end points, e.g. 20% weight loss.

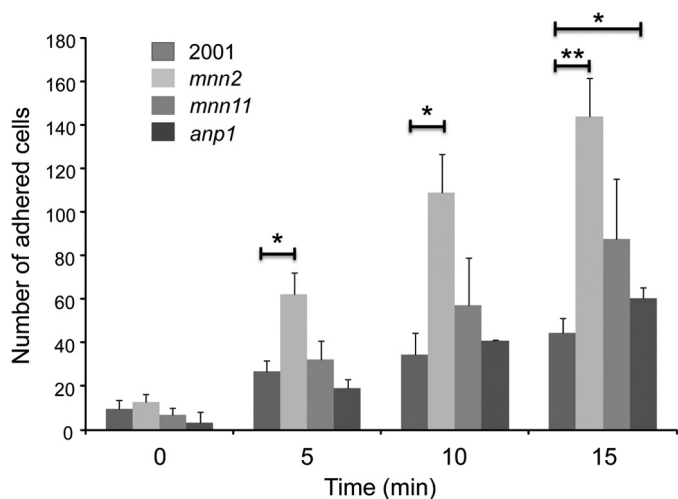


**FIGURE 8. *C. glabrata anp1* and *mnn2* are hyperadherent to HMEC-1 endothelial cells.** Adhesion of *C. glabrata* 2001, *anp1*, *mnn2*, and *mnn11* to HMEC-1 endothelial monolayers under conditions of shear flow. *C. glabrata* 2001, *anp1*, *mnn2*, and *mnn11* cells were perfused through a flow chamber over an HMEC-1 monolayer, and adhered cells were counted at 0-, 5-, 10-, and 15-min time points. *C. glabrata* cells were suspended at  $1.0 \times 10^6$  yeast/ml in Hanks' buffered salt solution and perfused over glass slides coated with confluent HMEC-1 monolayers, mounted in a parallel plate flow chamber. Adhesion events were visualized from a random field of view ( $0.15 \text{ mm}^2$ ) using a Zeiss Axiovert 200 M inverted fluorescence microscope. Images were then acquired over 15 min into a video file at 2 frames/min, and the total number of adherent cells/ $\text{mm}^2$  was recorded. All experiments were performed in a controlled environment chamber at  $37^\circ\text{C}$ , and each experiment was repeated with three separate confluent endothelial cell slides on at least two occasions. The results shown are the pooled triplicate data from a representative experiment, and the standard deviation indicated. \*,  $p < 0.05$ ; \*\*,  $p < 0.001$ , *t* test.

*C. glabrata mnn2* confirmed the lower level of mannosyl phosphorylation in this strain.

Our results indicate that *C. glabrata* 2001 has a mannan structure composed of  $\alpha$ -(1,6)-linked mannosyl backbone that has  $\alpha$ -(1,2)-linked mannosyl side chains that are the principal site of mannosyl phosphorylation and that some of these side chains terminate in  $\alpha$ -(1,3)-mannose residues. In *mnn2* cells, this is replaced by a structure that lacks  $\alpha$ -(1-2)-linked mannosyl side chains and exhibits severely depleted levels of phosphomannan (Fig. 9A). Whereas *anp1* and *mnn11* cells retain  $\alpha$ -(1-2)-linked mannosyl side chains and a greater degree of phosphomannan, they have shorter  $\alpha$ -(1-6)-linked mannosyl backbones (Fig. 9B). These structures are in broad agreement with the structures recently described in three different *C. glabrata* strains (20). Additionally, these overall changes in mannan structure very likely reflect differential glycosylation of individual proteins, many of which would have phenotypic implications. Functional analysis of these changes could be extremely revealing.

Changes in *C. albicans* mannan structure dramatically impact upon cell wall integrity, virulence, and activation of innate immunity (12, 36). Here, we have shown that deletion of *C. glabrata* mannosyltransferases again impacts cell wall integrity. We have previously shown that inactivation of *C. glabrata ACE2*, although not directly involved in modulating mannan structure, had a profound impact on the cell wall and secretome that results in massive overstimulation of host innate immunity and increases virulence almost 200-fold (48, 70, 71). We therefore sought to determine the impact of Anp1, Mnn2, and

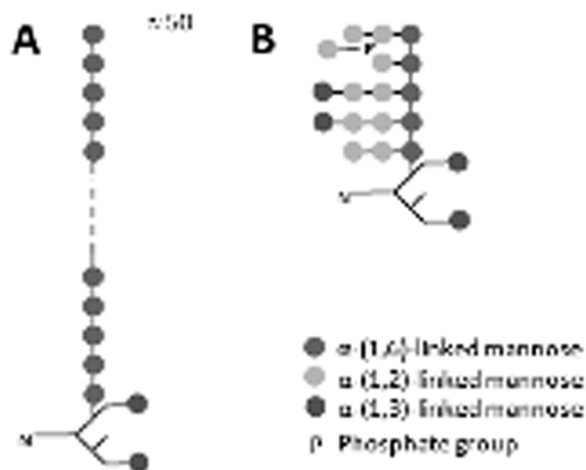


**FIGURE 9. Predicted mannan structures of *C. glabrata anp1*, *mnn2*, and *mnn11*.** A, predicted structure of the *C. glabrata mnn2* mannan as essentially a linear  $\alpha$ -(1,6)-mannan with minimal  $\alpha$ -(1,2)-linked side chain branching, and lacking the majority of mannosyl phosphorylation. B, predicted structure of *C. glabrata anp1* and *mnn11* mannans. These contain a shorter  $\alpha$ -(1,6)-mannan backbone; however, they retain secondary and tertiary side chain branching and some mannosyl phosphorylation. The precise structure of the secondary and tertiary branches is not known and is predicted from the mannan structural work described herein.

Mnn11 on virulence. In a mouse model of systemic candidosis, both the *C. glabrata anp1* and *mnn2* mutants were hypervirulent compared with wild-type *C. glabrata* 2001, whereas *C. glabrata mnn11* exhibits wild-type like virulence. *C. glabrata ace2* cells form large clumps, and hence it is possible that death is attributable to obstruction of the vasculature. However, in the experiments described here, mice were infected with single cells (*C. glabrata anp1*) or very small cellular aggregates (*C. glabrata mnn2* and *mnn11*,  $n < 5$ ) clearly demonstrating that increased virulence can occur in the absence of vascular occlusion. We predict that a septic shock-like response occurs in the *C. glabrata anp1*- and *mnn2*-infected mice, as has been observed in mice infected with other hypervirulent *C. glabrata* mutant strains (48, 72). Certainly, the balance between pro- and anti-inflammatory responses is important in many fungal infections (73). Potent activation of pattern recognition receptors can lead to septicemia and rising levels of pro-inflammatory cytokines such as TNF- $\alpha$  and IL-6, which can reflect the balance between inflammatory responses (74, 75). Cytokine analysis of the serum 24 h post-infection (four mice per group) was conducted to investigate this; however, the variation in absolute cytokine levels between mice was too high to allow comparison within such a small cohort. Hence, we have been unable to confirm or refute this prediction.

Another issue with respect to the virulence characteristics of *anp1* and *mnn11* strains needs to be addressed. In *S. cerevisiae*, Anp1 and Mnn11 are both members of the mannosyl polymerase II complex and either contribute to or exhibit  $\alpha$ -(1,6)-mannosyltransferase activity (76, 77). Our data strongly suggest that this function is conserved in *C. glabrata*. So the question arises, why do strains that lack components of the same enzyme complex exhibit different virulence levels? Especially as we have shown that the outer chain mannan structure is similar in *C. glabrata anp1* and *mnn11* strains (Fig. 9). To address this, we sought to determine whether variations in the ability to elicit

## Candida glabrata Glycosylation Mutants

immune activation *in vitro* or adherence to endothelial cells, both important mediators of the host-fungal interaction, could explain this variation. *mnn2*, *mnn11*, and *anp1* cells were hyper-elicitors of TNF- $\alpha$  production from RAW264.7 cells compared with *C. glabrata* 2001 (supplemental Fig. 1), suggesting that they are all capable of overactivation of innate immunity, at least *in vitro*, and hence this cannot explain the virulence difference.

The ability to adhere to cells is a prerequisite for tissue penetration, invasion, and disease progression, and many of the proteins that mediate this interaction are, or are likely to be, glycosylated (78–81). The crucial role of adhesion in *C. glabrata* pathogenesis has been demonstrated by the observation that the glycosylphosphatidylinositol-linked aspartyl proteases encoded by *YPS1-11* are essential for virulence (78–81). We therefore sought to determine whether the differences in virulence could be explained by differences in adherence. Most reported studies of *Candida* adhesion employ static assays where the fungal cells remain in prolonged contact with cultured monolayers (82–84). Flow assays more closely mimic the passing and brief interactions that *Candida* cells have with endothelial cells, under conditions of shear stress and flow that occur in blood vessels (64, 85). In this study we compared the adhesion capacity of *C. glabrata* 2001, *anp1*, *mnn2*, and *mnn11* strains to endothelial cells under conditions of shear flow. In this flow adhesion assay, only *C. glabrata mnn2* cells were convincingly hyper-adherent to endothelial cells, compared with the parent *C. glabrata* 2001 strain, although *anp1* cells were also statistically increased in their ability to adhere to HMEC-1 cells. Hence, there is no distinct difference in this crucial aspect of the host-pathogen interaction that can explain the difference in virulence seen between *anp1*, *mnn2*, and *mnn11* cells. It remains to be elucidated what, if any, other structural differences there are between *anp1/mnn2* and *mnn11* cells and how this subsequently affects the interaction with the host. However, it is possible to speculate that the glycosylation of specific adhesins may influence these interactions significantly (78–81).

Finally, we have shown that inactivation of *C. glabrata ANP1* and *MNN2* results in an increased ability to cause disease, whereas loss of *MNN11* has no impact on virulence. This is in contrast to *C. albicans*, and other fungi, where changes in the external glycan structure often result in attenuation. Hence, it is not prudent to draw predictions of what we may expect to observe in *C. glabrata* based upon studies in *C. albicans*. *C. glabrata* and *C. albicans* are not particularly closely related phylogenetically (57), and it is not surprising that they have different virulence traits. It is vitally important, with the growing incidence of this pathogen and its innate resistance to many currently available antifungal drugs, that we dissect virulence attributes directly in *C. glabrata*.

*Acknowledgment*—We are grateful to Xinfu Shi for technical support.

## REFERENCES

1. Wisplinghoff, H., Seifert, H., Tallent, S. M., Bischoff, T., Wenzel, R. P., and Edmond, M. B. (2003) Nosocomial bloodstream infections in pediatric patients in United States hospitals: epidemiology, clinical features, and susceptibilities. *Pediatr. Infect. Dis. J.* **22**, 686–691
2. Ruan, S. Y., Lee, L. N., Jerng, J. S., Yu, C. J., and Hsueh, P. R. (2008) *Candida glabrata* fungaemia in intensive care units. *Clin. Microbiol. Infect.* **14**, 136–140
3. Klis, F. M., Boersma, A., and De Groot, P. W. (2006) Cell wall construction in *Saccharomyces cerevisiae*. *Yeast* **23**, 185–202
4. Ruiz-Herrera, J., Elorza, M. V., Valentín, E., and Sentandreu, R. (2006) Molecular organization of the cell wall of *Candida albicans* and its relation to pathogenicity. *FEMS Yeast Res.* **6**, 14–29
5. Latgé, J. P. (2007) The cell wall: a carbohydrate armour for the fungal cell. *Mol. Microbiol.* **66**, 279–290
6. Netea, M. G., Brown, G. D., Kullberg, B. J., and Gow, N. A. (2008) An integrated model of the recognition of *Candida albicans* by the innate immune system. *Nat. Rev. Microbiol.* **6**, 67–78
7. Bowman, S. M., and Free, S. J. (2006) The structure and synthesis of the fungal cell wall. *BioEssays* **28**, 799–808
8. Netea, M. G., and Maródi, L. (2010) Innate immune mechanisms for recognition and uptake of *Candida* species. *Trends Immunol.* **31**, 346–353
9. Gow, N. A., Netea, M. G., Munro, C. A., Ferwerda, G., Bates, S., Mora-Montes, H. M., Walker, L., Jansen, T., Jacobs, L., Tsoni, V., Brown, G. D., Odds, F. C., Van der Meer, J. W., Brown, A. J., and Kullberg, B. J. (2007) Immune recognition of *Candida albicans*  $\beta$ -glucan by dectin-1. *J. Infect. Dis.* **196**, 1565–1571
10. van de Veerndonk, F. L., Kullberg, B. J., van der Meer, J. W., Gow, N. A., and Netea, M. G. (2008) Host-microbe interactions: innate pattern recognition of fungal pathogens. *Curr. Opin. Microbiol.* **11**, 305–312
11. Reid, D. M., Gow, N. A., and Brown, G. D. (2009) Pattern recognition: recent insights from Dectin-1. *Curr. Opin. Immunol.* **21**, 30–37
12. Mora-Montes, H. M., Bates, S., Netea, M. G., Castillo, L., Brand, A., Buurman, E. T., Díaz-Jiménez, D. F., Jan Kullberg, B., Brown, A. J., Odds, F. C., and Gow, N. A. (2010) A multifunctional mannosyltransferase family in *Candida albicans* determines cell wall mannan structure and host-fungus interactions. *J. Biol. Chem.* **285**, 12087–12095
13. Taylor, P. R., Tsoni, S. V., Willment, J. A., Dennehy, K. M., Rosas, M., Findon, H., Haynes, K., Steele, C., Botto, M., Gordon, S., and Brown, G. D. (2007) Dectin-1 is required for  $\beta$ -glucan recognition and control of fungal infection. *Nat. Immunol.* **8**, 31–38
14. Murciano, C., Moyes, D. L., Runglall, M., Islam, A., Mille, C., Fradin, C., Poulain, D., Gow, N. A., and Naglik, J. R. (2011) *Candida albicans* cell wall glycosylation may be indirectly required for activation of epithelial cell proinflammatory responses. *Infect. Immun.* **79**, 4902–4911
15. Gow, N. A., and Hube, B. (2012) Importance of the *Candida albicans* cell wall during commensalism and infection. *Curr. Opin. Microbiol.* **15**, 406–412
16. Dean, N. (1999) Asparagine-linked glycosylation in the yeast Golgi. *Biochim. Biophys. Acta* **1426**, 309–322
17. Kobayashi, H., Mitobe, H., Takahashi, K., Yamamoto, T., Shibata, N., and Suzuki, S. (1992) Structural study of a cell wall mannan-protein complex of the pathogenic yeast *Candida glabrata* IFO 0622 strain. *Arch. Biochem. Biophys.* **294**, 662–669
18. Kobayashi, H., Oyamada, H., Iwadata, N., Suzuki, H., Mitobe, H., Takahashi, K., Shibata, N., Suzuki, S., and Okawa, Y. (1998) Structural and immunochemical characterization of  $\beta$ -1,2-linked mannosyl phosphate residue in the cell wall mannan of *Candida glabrata*. *Arch. Microbiol.* **169**, 188–194
19. Okawa, Y., and Goto, K. (2006) Disappearance of antigenic factor 6 in *Candida glabrata* IFO 0622 strain cells cultured at high temperature. *Biol. Pharm. Bull.* **29**, 187–189
20. Takahashi, S., Kudoh, A., Okawa, Y., and Shibata, N. (2012) Significant differences in the cell-wall mannans from three *Candida glabrata* strains correlate with antifungal drug sensitivity. *FEBS J.* **279**, 1844–1856
21. Gemmill, T. R., and Trimble, R. B. (1999) Overview of N- and O-linked oligosaccharide structures found in various yeast species. *Biochim. Biophys. Acta* **1426**, 227–237
22. Knauer, R., and Lehle, L. (1994) The N-oligosaccharyltransferase complex from yeast. *FEBS Lett.* **344**, 83–86
23. Herscovics, A. (1999) Processing glycosidases of *Saccharomyces cerevisiae*

- siae*. *Biochim. Biophys. Acta* **1426**, 275–285
24. Nakayama, K., Nagasu, T., Shimma, Y., Kuromitsu, J., and Jigami, Y. (1992) *OCH1* encodes a novel membrane-bound mannosyltransferase: outer chain elongation of asparagine-linked oligosaccharides. *EMBO J.* **11**, 2511–2519
  25. Lussier, M., Sdicu, A. M., and Bussey, H. (1999) The KTR and MNN1 mannosyltransferase families of *Saccharomyces cerevisiae*. *Biochim. Biophys. Acta* **1426**, 323–334
  26. Rayner, J. C., and Munro, S. (1998) Identification of the MNN2 and MNN5 mannosyltransferases required for forming and extending the mannose branches of the outer chain mannans of *Saccharomyces cerevisiae*. *J. Biol. Chem.* **273**, 26836–26843
  27. Ballou, C. E. (1990) Isolation, characterization, and properties of *Saccharomyces cerevisiae* *mnn* mutants with nonconditional protein glycosylation defects. *Methods Enzymol.* **185**, 440–470
  28. Chapman, R. E., and Munro, S. (1994) The functioning of the yeast Golgi apparatus requires an ER protein encoded by *ANPI*, a member of a new family of genes affecting the secretory pathway. *EMBO J.* **13**, 4896–4907
  29. Häusler, A., and Robbins, P. W. (1992) Glycosylation in *Saccharomyces cerevisiae*: cloning and characterization of an  $\alpha$ -1,2-mannosyltransferase structural gene. *Glycobiology* **2**, 77–84
  30. Hill, K., Boone, C., Goebel, M., Puccia, R., Sdicu, A. M., and Bussey, H. (1992) Yeast *KRE2* defines a new gene family encoding probable secretory proteins, and is required for the correct N-glycosylation of proteins. *Genetics* **130**, 273–283
  31. Lussier, M., Sdicu, A. M., Bussereau, F., Jacquet, M., and Bussey, H. (1997) The Ktr1p, Ktr3p, and Kre2p/Mnt1p mannosyltransferases participate in the elaboration of yeast O- and N-linked carbohydrate chains. *J. Biol. Chem.* **272**, 15527–15531
  32. Lussier, M., Sdicu, A. M., Winnett, E., Vo, D. H., Sheraton, J., Dusterhöft, A., Storms, R. K., and Bussey, H. (1997) Completion of the *Saccharomyces cerevisiae* genome sequence allows identification of *KTR5*, *KTR6*, and *KTR7* and definition of the nine-membered *KRE2/MNT1* mannosyltransferase gene family in this organism. *Yeast* **13**, 267–274
  33. Romero, P. A., Lussier, M., Sdicu, A. M., Bussey, H., and Herscovics, A. (1997) Ktr1p is an  $\alpha$ -1,2-mannosyltransferase of *Saccharomyces cerevisiae*. Comparison of the enzymic properties of soluble recombinant Ktr1p and Kre2p/Mnt1p produced in *Pichia pastoris*. *Biochem. J.* **321**, 289–295
  34. Lussier, M., Sdicu, A. M., Camirand, A., and Bussey, H. (1996) Functional characterization of the *YURI*, *KTR1*, and *KTR2* genes as members of the yeast *KRE2/MNT1* mannosyltransferase gene family. *J. Biol. Chem.* **271**, 11001–11008
  35. Yip, C. L., Welch, S. K., Klebl, F., Gilbert, T., Seidel, P., Grant, F. J., O'Hara, P. J., and MacKay, V. L. (1994) Cloning and analysis of the *Saccharomyces cerevisiae* *MNN9* and *MNN1* genes required for complex glycosylation of secreted proteins. *Proc. Natl. Acad. Sci. U.S.A.* **91**, 2723–2727
  36. Bates, S., Hughes, H. B., Munro, C. A., Thomas, W. P., MacCallum, D. M., Bertram, G., Atrih, A., Ferguson, M. A., Brown, A. J., Odds, F. C., and Gow, N. A. (2006) Outer chain N-glycans are required for cell wall integrity and virulence of *Candida albicans*. *J. Biol. Chem.* **281**, 90–98
  37. Munro, C. A., Bates, S., Buurman, E. T., Hughes, H. B., MacCallum, D. M., Bertram, G., Atrih, A., Ferguson, M. A., Bain, J. M., Brand, A., Hamilton, S., Westwater, C., Thomson, L. M., Brown, A. J., Odds, F. C., and Gow, N. A. (2005) Mnt1p and Mnt2p of *Candida albicans* are partially redundant  $\alpha$ -1,2-mannosyltransferases that participate in O-linked mannosylation and are required for adhesion and virulence. *J. Biol. Chem.* **280**, 1051–1060
  38. Mora-Montes, H. M., Ponce-Noyola, P., Villagómez-Castro, J. C., Gow, N. A., Flores-Carreón, A., and López-Romero, E. (2009) Protein glycosylation in *Candida*. *Future Microbiol.* **4**, 1167–1183
  39. Olson, G. M., Fox, D. S., Wang, P., Alspaugh, J. A., and Buchanan, K. L. (2007) Role of protein O-mannosyltransferase Pmt4 in the morphogenesis and virulence of *Cryptococcus neoformans*. *Eukaryot. Cell* **6**, 222–234
  40. Willger, S. D., Ernst, J. F., Alspaugh, J. A., and Lengeler, K. B. (2009) Characterization of the PMT gene family in *Cryptococcus neoformans*. *PLoS One* **4**, e6321
  41. Kwon-Chung, K. J., and Rhodes, J. C. (1986) Encapsulation and melanin formation as indicators of virulence in *Cryptococcus neoformans*. *Infect. Immun.* **51**, 218–223
  42. Levitz, S. M., and Specht, C. A. (2006) The molecular basis for the immunogenicity of *Cryptococcus neoformans* mannoproteins. *FEMS Yeast Res.* **6**, 513–524
  43. Timpel, C., Strahl-Bolsinger, S., Ziegelbauer, K., and Ernst, J. F. (1998) Multiple functions of Pmt1p-mediated protein O-mannosylation in the fungal pathogen *Candida albicans*. *J. Biol. Chem.* **273**, 20837–20846
  44. Timpel, C., Zink, S., Strahl-Bolsinger, S., Schröppel, K., and Ernst, J. (2000) Morphogenesis, adhesive properties, and antifungal resistance depend on the Pmt6 protein mannosyltransferase in the fungal pathogen *Candida albicans*. *J. Bacteriol.* **182**, 3063–3071
  45. Jawhara, S., Mogensen, E., Maggiotto, F., Fradin, C., Sarazin, A., Dubuquoy, L., Maes, E., Guérardel, Y., Janbon, G., and Poulain, D. (2012) Murine model of dextran sulfate sodium-induced colitis reveals *Candida glabrata* virulence and contribution of  $\beta$ -mannosyltransferases. *J. Biol. Chem.* **287**, 11313–11324
  46. Hampsey, M. (1997) A review of phenotypes in *Saccharomyces cerevisiae*. *Yeast* **13**, 1099–1133
  47. Weig, M., Haynes, K., Rogers, T. R., Kurzai, O., Frosch, M., and Mühlischlegel, F. A. (2001) A GAS-like gene family in the pathogenic fungus *Candida glabrata*. *Microbiology* **147**, 2007–2019
  48. Kamran, M., Calcagno, A. M., Findon, H., Bignell, E., Jones, M. D., Warn, P., Hopkins, P., Denning, D. W., Butler, G., Rogers, T., Mühlischlegel, F. A., and Haynes, K. (2004) Inactivation of transcription factor gene *ACE2* in the fungal pathogen *Candida glabrata* results in hypervirulence. *Eukaryot. Cell* **3**, 546–552
  49. Reuss, O., Vik, A., Kolter, R., and Morschhäuser, J. (2004) The *SAT1* flipper, an optimized tool for gene disruption in *Candida albicans*. *Gene* **341**, 119–127
  50. Kitada, K., Yamaguchi, E., and Arisawa, M. (1996) Isolation of a *Candida glabrata* centromere and its use in construction of plasmid vectors. *Gene* **175**, 105–108
  51. Brachmann, C. B., Davies, A., Cost, G. J., Caputo, E., Li, J., Hieter, P., and Boeke, J. D. (1998) Designer deletion strains derived from *Saccharomyces cerevisiae* S288C: a useful set of strains and plasmids for PCR-mediated gene disruption and other applications. *Yeast* **14**, 115–132
  52. Gietz, R. D., and Sugino, A. (1988) New yeast-*Escherichia coli* shuttle vectors constructed with *in vitro* mutagenized yeast genes lacking six-base pair restriction sites. *Gene* **74**, 527–534
  53. Calcagno, A. M., Bignell, E., Rogers, T. R., Jones, M. D., Mühlischlegel, F. A., and Haynes, K. (2005) *Candida glabrata* Ste11 is involved in adaptation to hypertonic stress, maintenance of wild-type levels of filamentation and plays a role in virulence. *Med. Mycol.* **43**, 355–364
  54. Calcagno, A. M., Bignell, E., Rogers, T. R., Canedo, M., Mühlischlegel, F. A., and Haynes, K. (2004) *Candida glabrata* Ste20 is involved in maintaining cell wall integrity and adaptation to hypertonic stress, and is required for wild-type levels of virulence. *Yeast* **21**, 557–568
  55. Calcagno, A. M., Bignell, E., Warn, P., Jones, M. D., Denning, D. W., Mühlischlegel, F. A., Rogers, T. R., and Haynes, K. (2003) *Candida glabrata* *STE12* is required for wild-type levels of virulence and nitrogen starvation induced filamentation. *Mol. Microbiol.* **50**, 1309–1318
  56. MacCallum, D. M., Findon, H., Kenny, C. C., Butler, G., Haynes, K., and Odds, F. C. (2006) Different consequences of *ACE2* and *SWIS* gene disruptions for virulence of pathogenic and nonpathogenic yeasts. *Infect. Immun.* **74**, 5244–5248
  57. Dujon, B., Sherman, D., Fischer, G., Durrens, P., Casaregola, S., Lafontaine, I., De Montigny, J., Marck, C., Neuvéglise, C., Talla, E., Goffard, N., Franjeul, L., Aigle, M., Anthouard, V., Babour, A., Barbe, V., Barnay, S., Blanchin, S., Beckerich, J. M., Beyne, E., Bleykasten, C., Boisramé, A., Boyer, J., Cattolico, L., Confanioleri, F., De Daruvar, A., Despons, L., Fabre, E., Fairhead, C., Ferry-Dumazet, H., Groppi, A., Hantraye, F., Hennequin, C., Jauniaux, N., Joyet, P., Kachouri, R., Kerrest, A., Koszul, R., Lemaire, M., Lesur, I., Ma, L., Muller, H., Nicaud, J. M., Nikolski, M., Oztas, S., Ozier-Kalogeropoulos, O., Pellenz, S., Potier, S., Richard, G. F., Straub, M. L., Suleau, A., Swennen, D., Tekai, F., Wesolowski-Louvel, M., Westhof, E., Wirth, B., Zeniou-Meyer, M., Zivanovic, I., Bolotin-Fukuhara, M., Thierry, A., Bouchier, C., Caudron, B., Scarpelli, C., Gaillardin, C., Weissenbach, J., Wincker, P., and Souciet, J. L. (2004) Genome evolution in yeasts.

## Candida glabrata Glycosylation Mutants

- Nature* **430**, 35–44
58. Hobson, R. P., Munro, C. A., Bates, S., MacCallum, D. M., Cutler, J. E., Heinsbroek, S. E., Brown, G. D., Odds, F. C., and Gow, N. A. (2004) Loss of cell wall mannosylphosphate in *Candida albicans* does not influence macrophage recognition. *J. Biol. Chem.* **279**, 39628–39635
59. Kocourek, J., and Ballou, C. E. (1969) Method for fingerprinting yeast cell wall mannans. *J. Bacteriol.* **100**, 1175–1181
60. Lizicarova, I., Matulova, M., Capek, P., and Machova, E. (2007) Human pathogen *Candida dubliniensis*: A cell wall mannan with a high content of  $\beta$ -1,2-linked mannose. *Carbohydr. Pol.* **70**, 89–100
61. Ogawa, T., and Sasajima, K. (1981)  $^1\text{H}$ - and  $^{13}\text{C}$ -n.m.r.-spectral study of synthetic methyl D-manno-oligosaccharides. *Carbohydr. Res.* **97**, 205–227
62. Mueller, A., Raptis, J., Rice, P. J., Kalbfleisch, J. H., Stout, R. D., Ensley, H. E., Browder, W., and Williams, D. L. (2000) The influence of glucan polymer structure and solution conformation on binding to (1 $\rightarrow$ 3)- $\beta$ -D-glucan receptors in a human monocyte-like cell line. *Glycobiology* **10**, 339–346
63. Adams, E. L., Rice, P. J., Graves, B., Ensley, H. E., Yu, H., Brown, G. D., Gordon, S., Monteiro, M. A., Papp-Szabo, E., Lowman, D. W., Power, T. D., Wempe, M. F., and Williams, D. L. (2008) Differential high-affinity interaction of dectin-1 with natural or synthetic glucans is dependent upon primary structure and is influenced by polymer chain length and side-chain branching. *J. Pharmacol. Exp. Ther.* **325**, 115–123
64. Grubb, S. E., Murdoch, C., Sudbery, P. E., Saville, S. P., Lopez-Ribot, J. L., and Thornhill, M. H. (2009) Adhesion of *Candida albicans* to endothelial cells under physiological conditions of flow. *Infect. Immun.* **77**, 3872–3878
65. Shibata, N., Suzuki, A., Kobayashi, H., and Okawa, Y. (2007) Chemical structure of the cell-wall mannan of *Candida albicans* serotype A and its difference in yeast and hyphal forms. *Biochem. J.* **404**, 365–372
66. Shibata, N., Kobayashi, H., Okawa, Y., and Suzuki, S. (2003) Existence of novel  $\beta$ -1,2 linkage-containing side chain in the mannan of *Candida lusitanae*, antigenically related to *Candida albicans* serotype A. *Eur. J. Biochem.* **270**, 2565–2575
67. Kobayashi, H., Oyamada, H., Matsuda, K., Shibata, N., and Suzuki, S. (2003) Distribution of antigenic oligomannosyl side chains in the cell wall mannans of several strains of *Candida tropicalis*. *Arch. Microbiol.* **180**, 76–80
68. Ballou, L., Cohen, R. E., and Ballou, C. E. (1980) *Saccharomyces cerevisiae* mutants that make mannoproteins with a truncated carbohydrate outer chain. *J. Biol. Chem.* **255**, 5986–5991
69. Jigami, Y., and Odani, T. (1999) Mannosylphosphate transfer to yeast mannan. *Biochim. Biophys. Acta* **1426**, 335–345
70. Stead, D., Findon, H., Yin, Z., Walker, J., Selway, L., Cash, P., Dujon, B. A., Hennequin, C., Brown, A. J., and Haynes, K. (2005) Proteomic changes associated with inactivation of the *Candida glabrata* ACE2 virulence-moderating gene. *Proteomics* **5**, 1838–1848
71. Stead, D. A., Walker, J., Holcombe, L., Gibbs, S. R., Yin, Z., Selway, L., Butler, G., Brown, A. J., and Haynes, K. (2010) Impact of the transcriptional regulator, Ace2, on the *Candida glabrata* secretome. *Proteomics* **10**, 212–223
72. Findon, H. (2006) *Microbiology*. Ph.D. thesis, Imperial College London, London
73. Romani, L. (2004) Immunity to fungal infections. *Nat. Rev. Immunol.* **4**, 1–23
74. Cohen, J. (2002) The immunopathogenesis of sepsis. *Nature* **420**, 885–891
75. Janeway, C. A., Jr., and Medzhitov, R. (2002) Innate immune recognition. *Annu. Rev. Immunol.* **20**, 197–216
76. Jungmann, J., Rayner, J. C., and Munro, S. (1999) The *Saccharomyces cerevisiae* protein Mnn10p/Bed1p is a subunit of a Golgi mannosyltransferase complex. *J. Biol. Chem.* **274**, 6579–6585
77. Jungmann, J., and Munro, S. (1998) Multi-protein complexes in the cis Golgi of *Saccharomyces cerevisiae* with  $\alpha$ -1,6-mannosyltransferase activity. *EMBO J.* **17**, 423–434
78. Cormack, B. P., Ghorri, N., and Falkow, S. (1999) An adhesin of the yeast pathogen *Candida glabrata* mediating adherence to human epithelial cells. *Science* **285**, 578–582
79. Domergue, R., Castaño, I., De Las Peñas, A., Zupancic, M., Lockett, V., Hebel, J. R., Johnson, D., and Cormack, B. P. (2005) Nicotinic acid limitation regulates silencing of *Candida* adhesins during UTI. *Science* **308**, 866–870
80. Castaño, I., Pan, S. J., Zupancic, M., Hennequin, C., Dujon, B., and Cormack, B. P. (2005) Telomere length control and transcriptional regulation of subtelomeric adhesins in *Candida glabrata*. *Mol. Microbiol.* **55**, 1246–1258
81. Kaur, R., Ma, B., and Cormack, B. P. (2007) A family of glycosylphosphatidylinositol-linked aspartyl proteases is required for virulence of *Candida glabrata*. *Proc. Natl. Acad. Sci. U.S.A.* **104**, 7628–7633
82. Gale, C. A., Bendel, C. M., McClellan, M., Hauser, M., Becker, J. M., Berman, J., and Hostetter, M. K. (1998) Linkage of adhesion, filamentous growth, and virulence in *Candida albicans* to a single gene, *INT1*. *Science* **279**, 1355–1358
83. Staab, J. F., Bradway, S. D., Fidel, P. L., and Sundstrom, P. (1999) Adhesive and mammalian transglutaminase substrate properties of *Candida albicans* Hwp1. *Science* **283**, 1535–1538
84. Zhao, X., Oh, S. H., Cheng, G., Green, C. B., Nuessen, J. A., Yeater, K., Leng, R. P., Brown, A. J., and Hoyer, L. L. (2004) *ALS3* and *ALS8* represent a single locus that encodes a *Candida albicans* adhesin; functional comparisons between Als3p and Als1p. *Microbiology* **150**, 2415–2428
85. Glee, P. M., Cutler, J. E., Benson, E. E., Bargatze, R. F., and Hazen, K. C. (2001) Inhibition of hydrophobic protein-mediated *Candida albicans* attachment to endothelial cells during physiologic shear flow. *Infect. Immun.* **69**, 2815–2820